LUNAR PROPERTIES FROM TRANSIENT AND STEADY MAGNETIC FIELD MEASUREMENTS

PALMER DYAL and CURTIS W. PARKIN*
NASA-Ames Research Center, Moffett Field, Calif., U.S.A.

Abstract. The electrical conductivity of the lunar interior has been determined from magnetic field step transients measured on the lunar dark side. The simplest model which best fits the data is a spherically symmetric three layer model having a nonconducting outer crust of radial thickness $\approx 0.03\ R_{moon}$; an intermediate layer of thickness $\Delta R \approx 0.37\ R_{moon}$, with electrical conductivity $\sigma_1 \approx 3.5 \times 10^{-4}$ mhos/m; and an inner core of radius $R_2 \approx 0.6\ R_m$ with conductivity $\sigma_2 \approx 10^{-2}$ mhos/m. Temperatures calculated from these conductivities in the three regions for an example of an olivine Moon are as follows: crust, < 440 K; intermediate layer, ≈ 890 K; and core, ≈ 1240 K. The whole-moon relative permeability has been calculated from the measurements to be $\mu/\mu_0 = 1.03 \pm 0.13$. Remanent magnetic fields at the landing sites are $38 \pm 3\ \gamma$ at Apollo 12, 43 ± 6 and $103 \pm 5\ \gamma$ at two Apollo 14 sites separated by 1.1 km, and $6 \pm 4\ \gamma$ at the Apollo 15 site. Measurements show that the $38\ \gamma$ remanent field at the Apollo 12 site is compressed to $54\ \gamma$ by a solar wind pressure increase of 7×10^{-8} dynes/cm^2.

1. Introduction

Apollo magnetometers have been deployed on the lunar surface to study (1) permanent lunar magnetic fields, (2) magnetic fields induced in the Moon in response to large scale solar and terrestrial magnetic fields, and (3) interactions of the Moon and lunar fields with the solar wind. To date three magnetometers have been deployed on the lunar surface: a lunar surface magnetometer (LSM) at the Apollo 12 site in Oceanus Procellarum (19 November 1969), a lunar portable magnetometer (LPM) at Apollo 14 in Fra Mauro (5 February 1971), and another LSM at the Apollo 15 Hadley-Apennines site (31 July 1971).

The total magnetic field measured by the surface magnetometers is the vector sum of a combination of the following field contributions: the external (solar or terrestrial) 'driving' field, permanent and induced lunar fields, and fields associated with the Moon-plasma interaction in the solar wind. The lunar orbiting Explorer 35 magnetometer, when positioned outside the lunar cavity, makes simultaneous measurements of the external driving field alone. In this paper we analytically compare these external 'input' fields with surface 'output' fields to calculate remanent surface magnetic fields and properties of the lunar interior such as magnetic permeability, electrical conductivity, and temperature. Through correlation with solar wind spectrometer data, moreover, we study solar plasma interaction with a lunar surface remanent field.

Since the external driving magnetic field in the lunar environment can vary considerably with the lunar orbital position (see Figure 1), it is possible to study the various lunar properties separately through careful selection of data time periods. During times when the Moon is immersed in steady geomagnetic tail field, time-dependent induction fields and solar wind interaction fields are negligible, allowing investigation

* National Research Council Postdoctoral Associate.

Communication presented at the Conference on Lunar Geophysics, held between October 18–21, 1971, at the Lunar Science Institute in Houston, Texas, U.S.A.

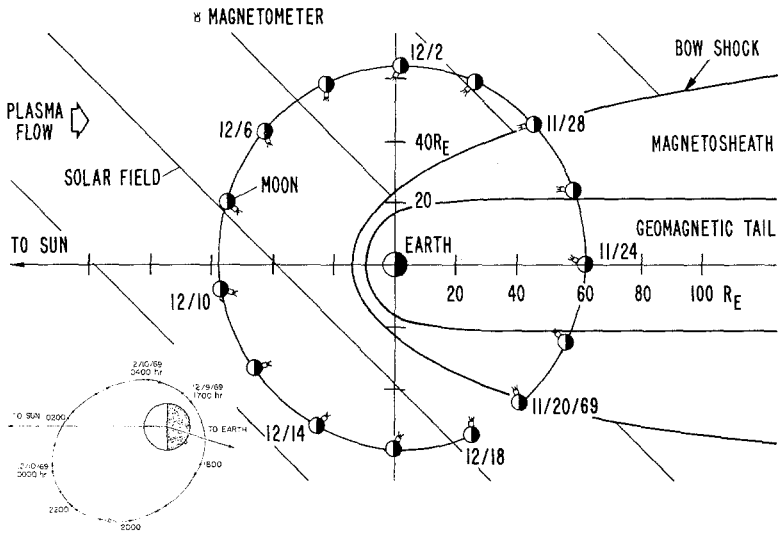

Fig. 1. Lunar orbit projection onto the solar ecliptic plane, showing the Apollo 12 magnetometer during the first post-deployment lunation, 1969. During a complete revolution around the earth, the magnetometer passes through the Earth's bow shock, the magnetosheath, the geomagnetic tail, and the interplanetary region dominated by solar plasma fields. The insert shows the Explorer 35 orbit around the Moon, projected onto the solar ecliptic plane. The Explorer 35 period of revolution is 11.5 hr.

of lunar permanent fields and time-independent magnetization ('soft perm') fields, the latter being functions of lunar magnetic permeability.

When the Moon is located in the free streaming solar wind, transients in the solar field induce lunar eddy current (poloidal) fields; measurements by a surface magnetometer on the nighttime side of the Moon can be used to analyze the poloidal field time-dependent decay characteristics. These decay characteristics are a function of interior electrical conductivity, which in turn is a strong function of temperature; therefore we can calculate a conductivity profile of the lunar interior and determine a corresponding temperature profile for assumed material compositions of the Moon.

When the Moon is located in the solar wind, the solar plasma will interact with lunar fields, provided they are of sufficient magnitude and extent. Thus a surface magnetometer located on the sunlit side in the presence of such a field will yield data which, when correlated with solar wind data, can be used to study the interaction. The 38-γ remanent field at Apollo 12 is found to be compressed by the solar wind.

2. Magnetic Fields at the Lunar Surface

During one revolution of the Moon around the Earth, there are several types of magnetic fields which in theory can contribute to the total field measured at the lunar surface. For reference we write the sum of these possible fields as

$$\mathbf{B}_A = \mathbf{B}_E + \mathbf{B}_S + \mathbf{B}_\mu + \mathbf{B}_P + \mathbf{B}_T + \mathbf{B}_D + \mathbf{B}_F, \tag{1}$$

where $\mathbf{B}_A$ is the total magnetic field measured on the surface by an Apollo lunar surface magnetometer (LSM); $\mathbf{B}_E$ is the total external (solar or terrestrial) driving magnetic field measured by the Explorer 35 and Apollo 15 subsatellite lunar orbiting magnetometers while outside the antisolar lunar cavity; $\mathbf{B}_S$ is the steady remanent field at the surface site; $\mathbf{B}_\mu$ is the magnetization field induced in permeable lunar material; $\mathbf{B}_P$ is the poloidal field caused by eddy currents induced in the lunar interior by changing external fields; $\mathbf{B}_T$ is the toroidal field corresponding to unipolar electrical currents driven through the Moon by the $\mathbf{V} \times \mathbf{B}_E$ electric field; $\mathbf{B}_D$ is the field associated with the diamagnetic lunar cavity; and $\mathbf{B}_F$ is the total field associated with the hydromagnetic solar wind flow past the Moon. It is noted that the fields of Equation (1) can also be classed as external ($\mathbf{B}_E$), permanent ($\mathbf{B}_S$), induced ($\mathbf{B}_\mu$, $\mathbf{B}_P$, $\mathbf{B}_T$), and solar wind interaction fields ($\mathbf{B}_D$, $\mathbf{B}_F$).

During one complete lunar orbit around the Earth, the electromagnetic environment of the Moon varies considerably with the lunar position (Figure 1). The relative importance of the fields in Equation (1) also varies with orbital position, and therefore different magnetic fields can be investigated during different times of each lunation.

When the Moon is passing through the geomagnetic tail, the ambient plasma-particle density is significantly reduced and the plasma-associated terms $\mathbf{B}_T$, $\mathbf{B}_D$, and $\mathbf{B}_F$ can be neglected. In quiet regions of the tail, $\mathbf{B}_E$ is constant, and the eddy current induction field $\mathbf{B}_P \to 0$. Equation (1) then reduces to

$$\mathbf{B}_A = \mathbf{B}_E + \mathbf{B}_\mu + \mathbf{B}_S . \tag{2}$$

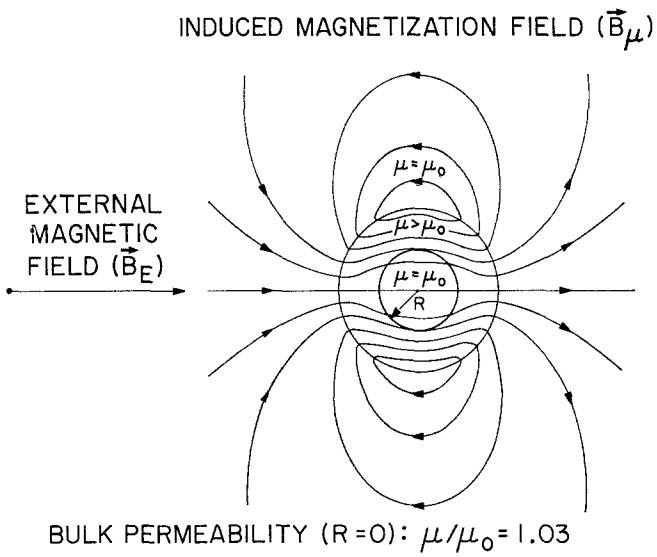

Fig. 2. Induced magnetization field $\mathbf{B}_\mu$. When a hypothetical global permeable shell is immersed in a uniform external magnetic field $\mathbf{B}_E$ (the outer portion of the Moon in the steady geomagnetic tail field in our case), a dipolar magnetic field $\mathbf{B}_\mu$ is induced which is axially aligned with $\mathbf{B}_E$. The net effect is that the total field $\mathbf{B}_E + \mathbf{B}_\mu$ tends to diminish in the nonpermeable core and concentrate in the shell.

The magnetization field $\mathbf{B}_\mu$ (Figure 2) is proportional to the external driving field $\mathbf{B}_E$: i.e.,

$$\mathbf{B}_A = (1 + K)\,\mathbf{B}_E + \mathbf{B}_S \tag{3}$$

(the proportionality constant K in turn depends upon the permeability and the dimensions of the permeable region of the Moon); therefore when the tail field $\mathbf{B}_E$ is zero (e.g., during neutral sheet crossings), $\mathbf{B}_A = \mathbf{B}_S$ and the Apollo magnetometer measures the steady remanent field alone. After $\mathbf{B}_S$ has been determined, the equation can be solved for the proportionality constant K, and the magnetic permeability μ can be calculated. Alternately, data for the vector components of $\mathbf{B}_A$ can be plotted versus components of $\mathbf{B}_E$; then K can be determined from curve slopes and the components of $\mathbf{B}_S$, from curve intercepts.

During times when the LSM is located on the dark (antisolar) side of the Moon, another combination of terms in Equation (1) can be neglected to a first approximation. While in the darkside cavity, the LSM is isolated from the plasma flow; hydromagnetic

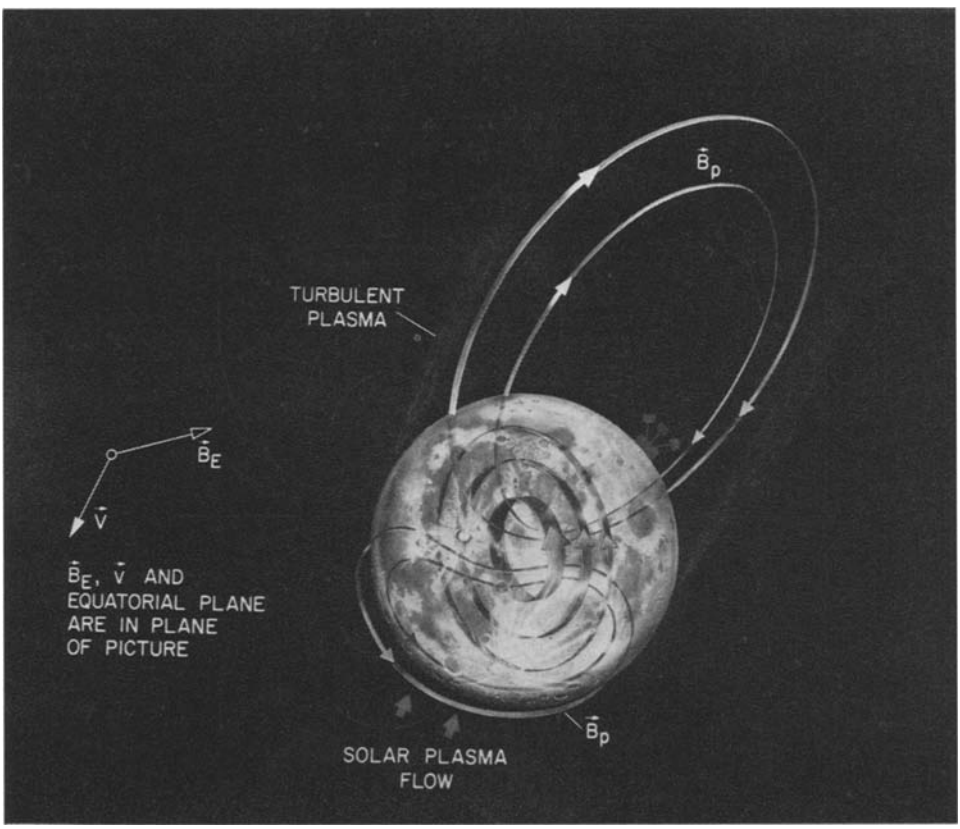

Fig. 3. Induced eddy-current magnetic field $\mathbf{B}_P$. A poloidal field $\mathbf{B}_P$ is induced by time-dependent fluctuations in the solar wind magnetic field. The lunar equatorial plane, the solar magnetic field $\mathbf{B}_E$, and the velocity $\mathbf{V}$ of the Moon with respect to the solar wind are in the plane of the page.

effects such as surface field compression by the solar wind will not occur and $\mathbf{B}_F$ can be disregarded. Subsequent analysis will show that the bulk lunar magnetic permeability is close to that of free space, and $\mathbf{B}_\mu$ is henceforth neglected. From time series step transient analysis, $\mathbf{B}_T$ and $\mathbf{B}_D$ have been found to be negligible (Dyal and Parkin, 1971a) compared to the eddy current induction field $\mathbf{B}_P$ (Figure 3) and Equation (1) reduces to

$$\mathbf{B}_A = \mathbf{B}_P + \mathbf{B}_E + \mathbf{B}_S . \tag{4}$$

After $\mathbf{B}_S$ has been calculated using Equation (3), only the poloidal field $\mathbf{B}_P$ is unknown. Equation (4) can then be solved for certain assumed lunar models, and curve fits of data to the solution determine the model dependent conductivity profile $\sigma(R)$. Furthermore, electrical conductivity is related to temperature, and the lunar interior temperature can be calculated for assumed lunar material compositions.

A different set of field terms in Equation (1) is dominant for surface magnetometer data obtained during lunar daytime; $\mathbf{B}_D \to 0$ outside the cavity, and the global fields $\mathbf{B}_\mu$ and $\mathbf{B}_T$ can again be neglected in comparison to $\mathbf{B}_P$ because of empirical findings, as noted previously. For the lunar daytime data, the surface magnetometer is exposed directly to the solar wind (Snyder *et al.*, 1970) and the associated wave modes and plasma field interaction effects; therefore the interaction term $\mathbf{B}_F$ is not to be assumed negligible in general, and Equation (1) becomes

$$\mathbf{B}_A = \mathbf{B}_P + \mathbf{B}_E + \mathbf{B}_S + \mathbf{B}_F . \tag{5}$$

The interaction field $\mathbf{B}_F$ has been found to be important during times of high solar wind particle density; at the Apollo 12 site, the local 38-γ remanent field is compressed

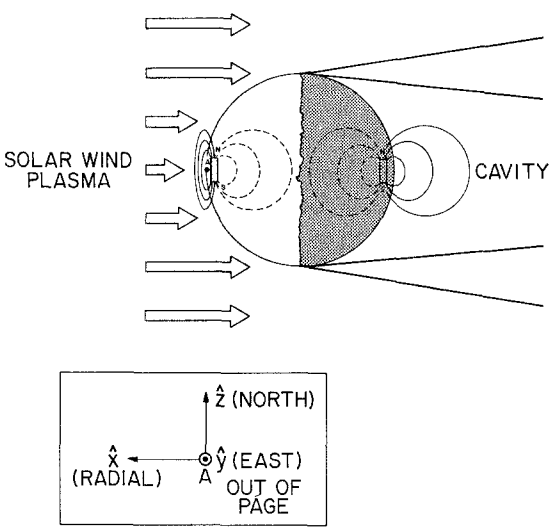

Fig. 4. Compression of a local remanent magnetic field by a high-density solar wind plasma. The remanent field is unperturbed during lunar night (antisolar side), while on the sunlit side the horizontal components are compressed. The insert shows the coordinate system used in this paper.

by high pressure plasma flow as shown conceptually in Figure 4. Plasma properties must therefore be taken into account for analysis of lunar daytime magnetometer data.

3. Descriptions of the Lunar Magnetometers

Magnetic fields at the lunar surface have been measured by magnetometers emplaced by astronauts on the Apollo 12, 14 and 15 missions. The three orthogonal vector components are measured as a function of time and position and telemetered to Earth. Simultaneously a magnetometer in the lunar orbiting Explorer 35 spacecraft measures the ambient solar and terrestrial field and transmits this information to Earth. Three different types of lunar magnetometers are described in the following paragraphs. Both a portable and stationary surface magnetometer are planned for the Apollo 16 mission to Descartes.

A. STATIONARY LUNAR SURFACE MAGNETOMETER (LSM)

The stationary magnetometer developed for the Apollo 12 and 15 missions is shown

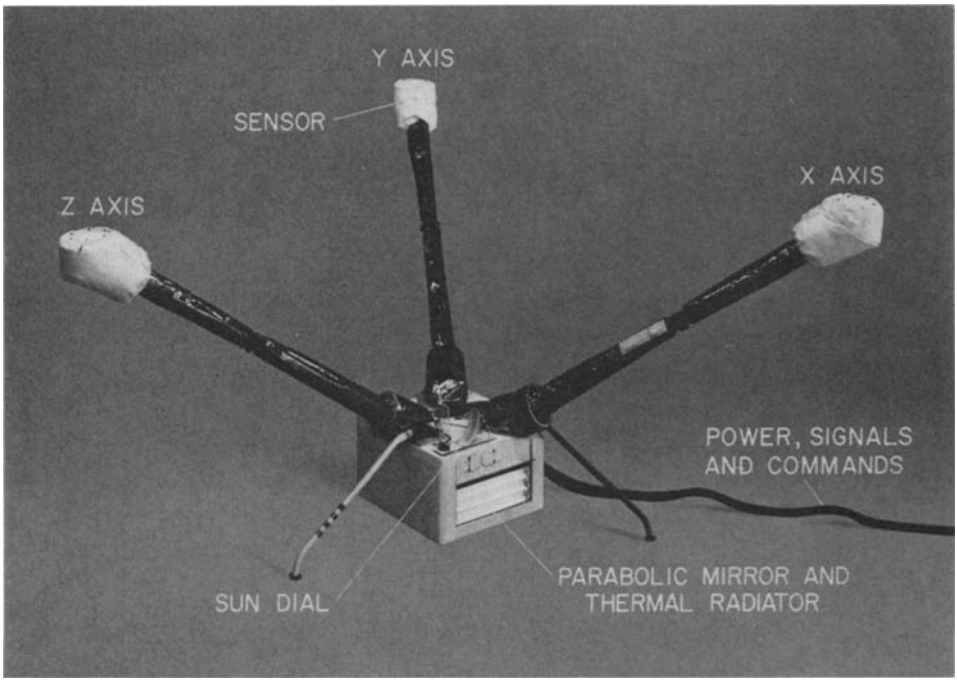

Fig. 5. Lunar surface magnetometer (LSM) deployed in the laboratory. The sensors are at the top end of the booms and approximately 75 cm above the ground. The electronics and motor drive assembly are located in the box, encased in a thermal blanket. Heat rejection during lunar day and retention during lunar night are controlled by a parabolic reflector array on two sides of the electronics box. The astronaut bubble level and azimuthal shadowgraph are shown on top of the box. Power, digital signals and commands are provided through the ribbon cable which connects to the ALSEP central station telemetry receiver and transmitter.

in Figure 5, and the instrument characteristics are given in Table I. A more detailed description of the instrument is reported by Dyal *et al.* (1970a).

The three orthogonal vector components of the magnetic field are measured by three fluxgate sensors (Geyger, 1964; Gordon *et al.*, 1965) located at the ends of three 100-cm-long orthogonal booms. The sensors are separated from each other by 150 cm and are 75 cm above the ground. Prelaunch test results show that magnetic fields due to artificial sources are less than 0.2 γ at the sensor locations. The instrument geometry as seen in Figure 5 is such that each sensor is directed approximately 35° above the horizontal with the Z-sensor pointed toward the east, the X-sensor toward the northwest, and the Y-sensor completing a right hand orthogonal system. Orientation measurements with respect to lunar coordinates are made with two devices. A shadowgraph is used by the astronaut to align and measure the azimuthal orientation with respect to the Moon-to-Sun line to an accuracy of 0.5°. Gravity level sensors measure the tilt angle to an accuracy of 0.2° every 4.8 s.

TABLE I

Apollo magnetometer characteristics

Parameter	Apollo 12 LSM	Apollo 15 LSM	Apollo 14 LSM
Ranges, γ	0 to ± 400 0 to ± 200 0 to ± 100	0 to ± 200 0 to ± 100 0 to $\pm$ 50	0 to ± 100 0 to $\pm$ 50
Resolution, γ	0.2	0.1	0.5
Frequency response, Hz	dc to 3	dc to 3	dc to 0.01
Angular response	Proportional to cosine of angle between magnetic field vector and sensor axis.		
Sensor geometry	3 orthogonal sensors at ends of 100 cm booms	3 orthogonal sensors at ends of 100 cm booms	3 orthogonal sensors in 6 cm cube
Analog zero determination	180° flip of sensor	180° flip of sensor	180° flip of sensor
Power, W	3.5	3.5	1.5
Weight, kg	8.9	8.9	4.6
Size, cm	$25 \times 28 \times 63$	$25 \times 28 \times 63$	$56 \times 15 \times 14$
Operating temperature °C	-50 to $+85$	-50 to $+85$	-30 to $+60$

The LSM can also be used as a gradiometer by sending commands to operate three motors in the instrument which rotate the sensors such that all simultaneously align parallel first to one of the other two boom axes, then to each of the other two boom axes in turn. This rotating alignment permits the vector gradient to be calculated in the plane of the sensors and also permits an independent measurement of the magnetic field vector at each sensor position.

Long term stability is attained by extensive use of digital circuitry, by internal calibration of the analog portion of the LSM every 18 hr, and by mechanical rotation

of each sensor through 180° in order to determine the sensor zero offset. The analog output of the sensor electronics is internally processed by a low-pass digital filter and a telemetry encoder; the output is transmitted to Earth via the central station *S*-band transmitter.

The LSM has two data samplers: the analog-to-digital converter (26.5 samples/s) and the central station telemetry encoder (3.3 samples/s). The prealias filter following the sensor electronics had attenuations of 3 *dB* at 1.7 Hz, 64 *dB* at 26.5 Hz, and 58 *dB* at the Nyquist frequency (13.2 Hz), with an attenuation rate of 22 *dB*/octave. The four pole Bessel digital filter limits the alias error to less than 0.05% and has less than 1% overshoot for a step function response. This filter has an attenuation of 3 *dB* at 0.3 Hz and 48 *dB* at the telemetry sampling Nyquist frequency (1.6 Hz), and it has a phase response that is linear with frequency. The response of the entire LSM measure-

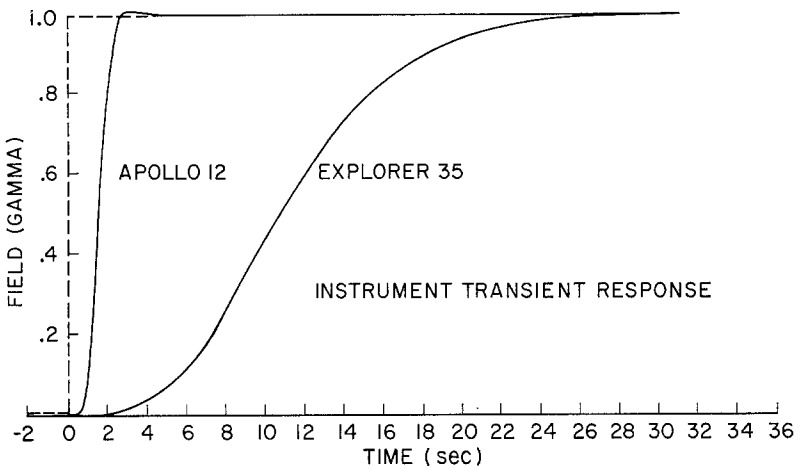

Fig. 6. Laboratory measurements comparing responses of the Apollo 12 and 15 and Explorer 35 magnetometers to a 1.0-γ magnetic step input.

ment system to a step-function input is shown in Figure 6. The digital filter can be bypassed by ground command in order to pass on higher frequency information.

B. LUNAR PORTABLE MAGNETOMETER (LPM)

The portable magnetometer developed for the Apollo 14 mission to Fra Mauro is shown in Figure 7, and the instrument characteristics are given in Table I. A more detailed description of the instrument is reported by Dyal *et al.* (1971).

The instrument was designed to be a totally self-contained, portable experiment package. Three orthogonally oriented fluxgate sensors are mounted on the top of a tripod, positioned 75 cm above the lunar surface. These sensors are connected by a 15-m-long cable to an electronics box which contains a battery, electronics and three milliammeters used to read the field output. The sensor tripod has a bubble level and shadowgraph which are used by the astronaut to align the device along the Moon-Sun

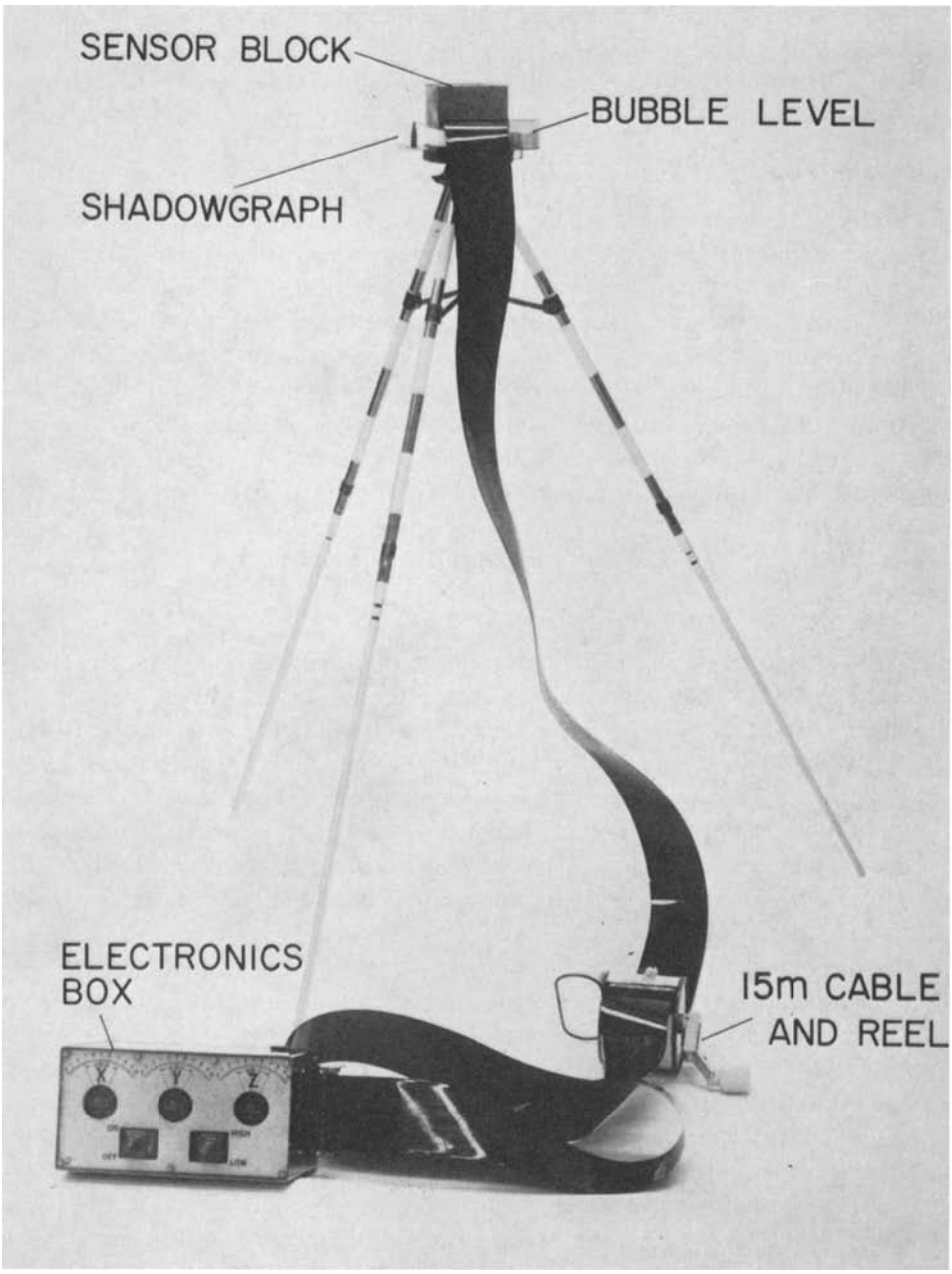

Fig. 7. Lunar portable magnetometer (LPM) deployed in the laboratory.

line to within 3°. The astronaut also rotates the sensor assembly 180° about a horizontal axis and 180° about a vertical axis in order to measure the zero offset for each axis. The instrument is designed to measure the time independent remanent fields and has an overall low-pass filter frequency response with a 3 *dB* point at 0.05 Hz. The readings (verbally relayed to Earth by the astronaut) are therefore independent of rapid fluctuations in the ambient solar wind field.

C. LUNAR ORBITING EXPLORER 35 MAGNETOMETER

The ambient steady state and time dependent magnetic fields in the lunar environment are measured by the Explorer 35 satellite magnetometer. The satellite, launched in July 1967, has an orbital period of 11.5 h, aposelene of 9390 km, and periselene of 2570 km (see Figure 1 insert). The Explorer 35 magnetometer measures three magnetic field vector components every 6.14 s and has an alias filter with 18 *dB* attenuation at the Nyquist frequency (0.08 Hz) of the spacecraft data sampling system. This instrument has a phase shift linear with frequency, and its step function response is slower than that of the Apollo 12 and 15 instruments (see Figure 6). A more detailed description of the instrument is reported by Sonett *et al.* (1967).

4. Transient Magnetic Field Measurements

A. LUNAR INTERNAL ELECTRICAL CONDUCTIVITY

Analysis of magnetic step transient measurements obtained while the surface magnetometer was on the lunar dark side has provided a means of calculating electrical conductivity and temperature profiles of the interior of the Moon (Dyal and Parkin, 1971b). As depicted in Figure 8 the Moon responds to a sudden magnetic field change in a manner similar to an electrically conducting sphere. The magnetic fields due to electrical eddy currents, according to Lenz's law, are induced in such a direction as to oppose the change in the external magnetic field. For data taken on the lunar dark side, the surface magnetometer is isolated from the plasma flow, and hydromagnetic effects can be disregarded.

Over one hundred step-transient fields which have penetrated the Moon have been analyzed using Apollo 12 lunar surface magnetometer dark side data and simultaneous data from the lunar orbiting Explorer 35 magnetometer. These data show that the Moon's response is similar to the eddy current response of a conducting sphere in a vacuum: measured surface magnetic field radial components have a damped response to solar wind field step transients, while components tangent to the lunar sphere have rapid response and overshoot initially, followed by decay to a steady state value.

The simplest lunar model which qualitatively explains the data is a three-layer conductivity model. A schematic of the response of this three-layered moon to a moving solar field discontinuity is shown in Figure 8. This figure shows that eddy-current fields, which are induced in the lunar interior upon arrival of the solar field transient, tend to retain the pretransient field configuration in the conducting interior regions. These eddy-current fields decay at a rate which is a function of interior

conductivity; the core has highest conductivity and core eddy currents persist longest. Eventually the post-transient solar field penetrates the entire lunar sphere.

Following the method of Smythe (1950), we have solved Maxwell's equations for eddy current transient response of a homogeneous sphere. We consider here the case where an external field step transient of magnitude $\Delta\mathbf{B}_E = \mathbf{B}_{Ef} - \mathbf{B}_{Eo}$ is applied to the lunar sphere at time $t=0$. The solutions for the components of the vector field

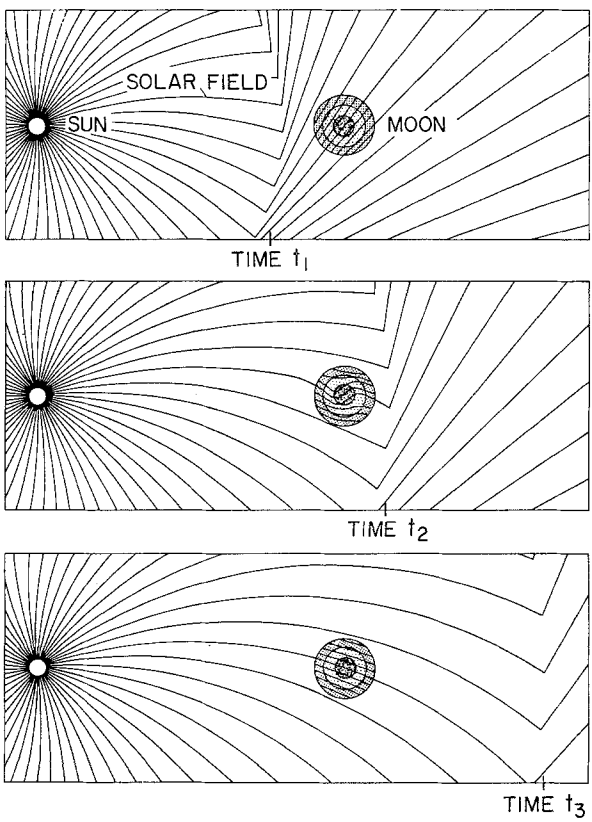

Fig. 8. Transient magnetic response of a three-layer conductivity model of the Moon for a case in which a directional discontinuity in the solar wind magnetic field travels outward past the Moon. The three layers are characterized by successively increasing electrical conductivity with depth into the Moon. Eddy currents persist in the deep core region of highest conductivity, causing the original field configuration to be preserved longest in that region.

measured on the lunar surface ($\mathbf{B}_A = \mathbf{B}_P + \mathbf{B}_E + \mathbf{B}_S$) can be expressed as follows for the radial and tangential components, respectively (Dyal and Parkin, 1971b);

$$B_{Ax} = -3\left(\frac{R_1}{R_m}\right)^3 (\Delta B_{Ex})\, F(t) + B_{Ex} + B_{Sx}, \tag{6}$$

$$B_{Ay,z} = \frac{3}{2}\left(\frac{R_1}{R_m}\right)^3 (\Delta B_{Ey,z})\, F(t) + B_{Ey,z} + B_{Sy,z}, \tag{7}$$

where $\Delta B_{Ei}=B_{Eif}-B_{Eio}$, $i=x, y, z$, and R_1 and R_m are radii of the conducting core and the Moon, respectively. The initial and final external applied field components are B_{Eio} and B_{Eif}, respectively, and are both measured by Explorer 35. Total surface fields measured by the Apollo 12 LSM are B_{Ai}, and the time dependence of the magnetic field is expressed as

$$F(t)=\frac{2}{\pi^2}\sum_{s=1}^{\infty}\frac{1}{s^2}\exp\left(\frac{-s^2\pi^2 t}{\mu_0\sigma_1 R_1^2}\right). \tag{8}$$

Solutions for Equations (6) and (7) for radial and tangential transients are shown graphically in Figure 9.

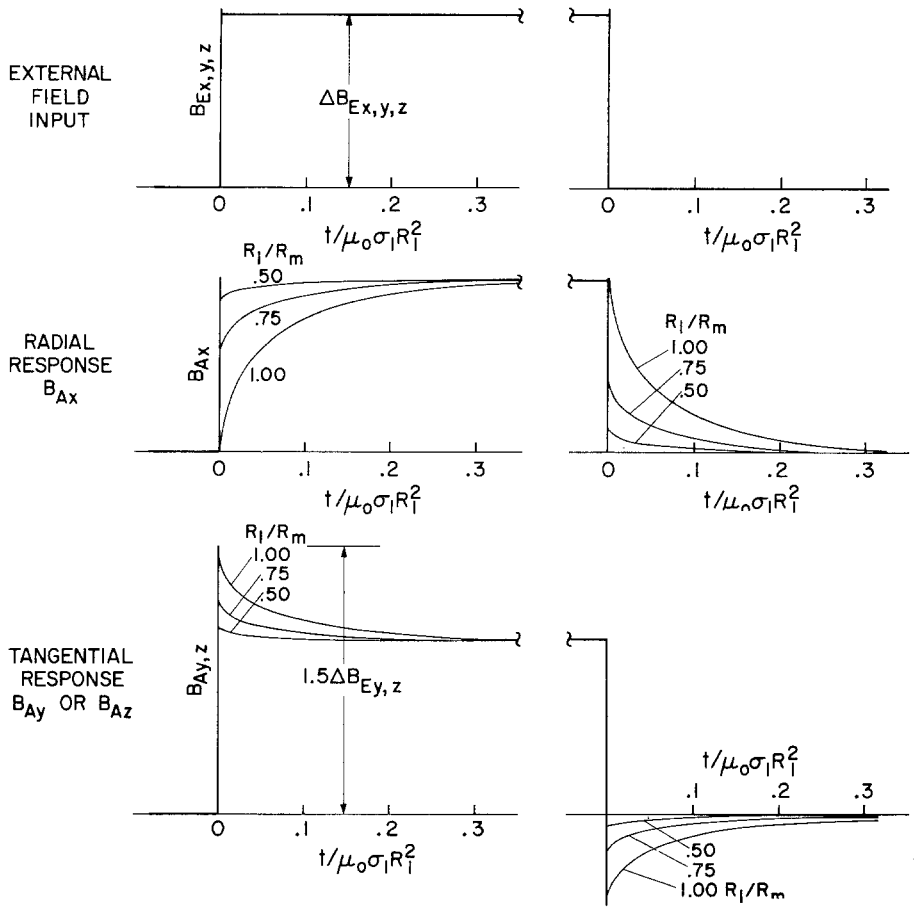

Fig. 9. Theoretical solutions for the lunar night vacuum poloidal magnetic field response of a homogeneous conducting lunar core of radius R_1 to a step function transient in the driving solar-wind magnetic field. For a step-function change $\Delta\mathbf{B}_E$ in the external driving field (measured by Explorer 35), the total magnetic field at the surface of the Moon $\mathbf{B}_A$ (measured by the Apollo 12 and 15 magnetometers) will be damped in the radial (B_{Ax}) component and will overshoot in the tangential (B_{Ay} and B_{Az}) components. The initial overshoot magnitude is limited to a maximum value $\Delta B_{Ey}/2$ or $\Delta B_{Ez}/2$ for the case $R_1 \to R_m$. A family of curves is shown for different values of the parameter R_1/R_m.

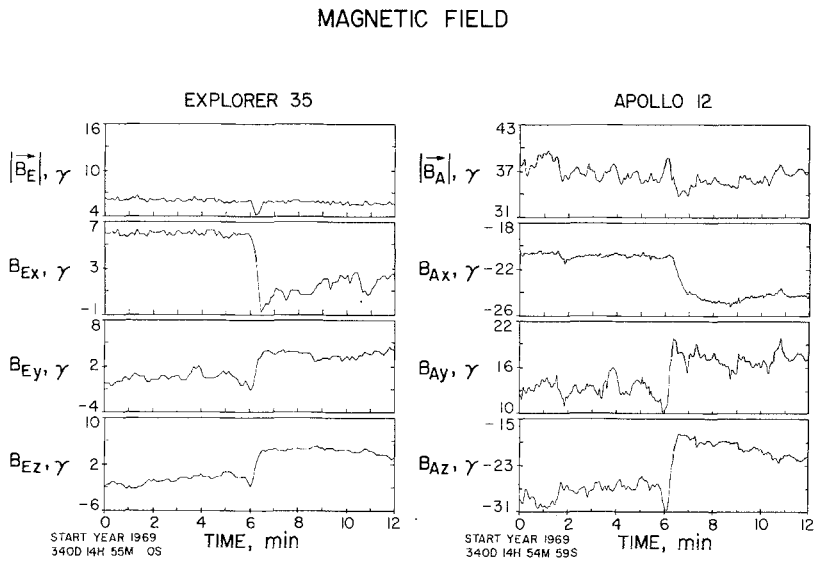

Fig. 10. Response to step function transients in all three vector components. The components are expressed in an ALSEP coordinate system, which originates on the lunar surface at the Apollo 12 site. The $\hat{x}$-axis is directly radially outward from the lunar surface; $\hat{y}$ and $\hat{z}$ are tangential to the surface, directed eastward and northward, respectively. Damping on the radial x-axis and overshoot on the tangential y- and z-axes are apparent. Apollo 12 and Explorer 35 data vertical scales differ because of the existence of a 38 ± 3-γ steady field at the Apollo 12 site.

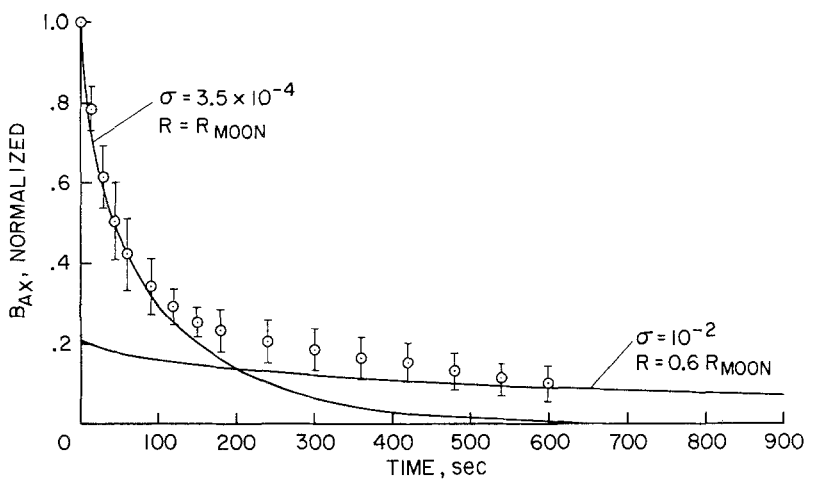

Fig. 11. Normalized transient response data, showing decay characteristics of the radial component of the total surface field B_{Ax} after arrival of a step transient which reduces the external magnetic field radial component by an amount ΔB_{Ex}, here normalized to one. The two curves are theoretical solutions of Equation (6) for two homogeneous cases, showing that the data fit a homogeneous model of the whole Moon of conductivity 3.5×10^{-4} mhos/m during early times after transient arrival ($t = 0$) and approach the homogeneous core solution ($\sigma = 10^{-2}$ mhos/m) for later times.

A typical example of a step transient event in Apollo 12 and Explorer 35 data is shown in Figure 10, and qualitative agreement between theory and data is easily seen. A more thorough analysis has shown that the data better fit a three-layer model (Dyal and Parkin, 1971b). The lunar response has been found not to be a function of position within a region of 400 km inside the optical shadow; therefore effects of solar wind hydromagnetic flow past the Moon are neglected. The lunar response is also independent of the Explorer 35 orbital position; eight step transient events have been analyzed for times when the Explorer 35 and Apollo 12 magnetometers were simultaneously inside the cavity, and the response is the same as for cases where Explorer 35 is outside the cavity.

Figure 11 is a plot of normalized data from eleven radial component step transients. To first order these points can be asymptotically fiit with a homogeneous core of radius 0.6 R_m with conductivity 10^{-2} mhos/m and an intermediate layer, bounded by radii 0.6 R_m and 0.97 R_m, of conductivity 3.5×10^{-4} mhos/m. An upper limit on the electrical conductivity of the outer crust is estimated to be 10^{-9} mhos/m (Dyal and Parkin, 1971a).

B. LUNAR INTERNAL TEMPERATURE

The electrical conductivity values obtained by measuring the time response characteristics of the vector magnetic field transient can be used to calculate the internal temperature distribution if the material composition is known. For materials that have been used to model the lunar interior (see, e.g., Urey and MacDonald, 1970; Kopal, 1969), the electrical conductivities are expressed as function of temperature by Nagata *et al.* (1970) by

$$\sigma_{\text{olivine}} = 55 \exp(-0.92/kT) + 4 \times 10^7 \exp(-2.7/kT)\,(\text{ohm} - \text{m})^{-1},$$
$$\sigma_{\text{peridotite}} = 3.8 \exp(-0.81/kT) + 10^7 \exp(-2.3/kT)\,(\text{ohm} - \text{m})^{-1}.$$

These conductivities are assumed to be independent of pressure below 50 kb (England *et al.*, 1968) and independent of frequency below 10 Hz (Keller and Frischknecht, 1966). A lunar cross section showing a temperature conductivity profile of a three-layer lunar interior is given in Figure 12.

5. Steady Magnetic Field Measurements

A. RELATIVE MAGNETIC PERMEABILITY OF THE LUNAR INTERIOR

During times when the Moon is immersed in steady regions of the geomagnetic tail, Equations (2) and (3) apply. Solutions for the spherically symmetric case illustrated in Figure 2, in terms of local ALSEP surface coordinates ($\hat{x}$, $\hat{y}$, $\hat{z}$) described earlier, are as follows (Jackson, 1962; Dyal and Parkin, 1971a):

$$\mathbf{B}_{Ax} = (1 + 2F)\,\mathbf{B}_{Ex} + \mathbf{B}_{Sx}, \tag{9}$$

$$\mathbf{B}_{Ay,z} = (1 - F)\,\mathbf{B}_{Ey,z} + \mathbf{B}_{Sy,z}, \tag{10}$$

where

$$F = \frac{(2k_m + 1)(k_m - 1)\left[1 - \left(\frac{R}{R_m}\right)^3\right]}{(2k_m + 1)(k_m + 2) - 2\left(\frac{R}{R_m}\right)^3 (k_m - 1)^2}. \tag{11}$$

In this equation, k_m is the relative permeability μ/μ_0; R_m is the lunar radius; and R is the radius of the boundary which encloses lunar material with temperature above the Curie point.

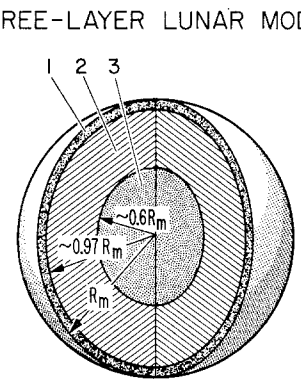

REGION	ELECTRICAL CONDUCTIVITY, σ, mhos/meter	TEMPERATURE, K		
		OLIVINE	PERIDOTITE	APOLLO 11 SURFACE SAMPLE
1	$<10^{-9}$	<440	<430	<300
2	$\sim 3.5\times10^{-4}$	890	1000	580
3	$\sim 10^{-2}$	1240	1270	740

Fig. 12. Conductivity (σ) and temperature contours for a three-layer Moon. Temperature calculations are based on σ as a function of temperature for pure olivine and peridotite (England *et al.*, 1968) and an Apollo 11 surface sample (Nagata *et al.*, 1970).

Figure 13(a) shows a plot of radial components of Apollo 12 LSM fields (B_{Ax}) versus the geomagnetic tail field (B_{Ex}) measured by Explorer 35. A least squares fit and slope calculations determine the factor $F = 1.2 \pm 0.5 \times 10^{-2}$, which is used to determine the relative magnetic permeability for an assumed inner radius R, as shown in Figure 13(b). For the bulk permeability of the Moon (the case $R=0$), $\mu/\mu_0 = 1.03 \pm 0.13$. For a thinner permeable shell inside the Moon, the permeability is higher, e.g., $\mu/\mu_0 = 1.05$ for $R/R_m = 0.6$ and $\mu/\mu_0 = 1.24$ for $R/R_m = 0.95$.

B. REMANENT MAGNETIC FIELDS AT THE APOLLO SITES

Local permanent fields $\mathbf{B}_S$ at four sites have been calculated, during times when the

Moon is located in quiet regions of the geomagnetic tail, by least-squares fits of measurements to Equations (9) and (10). Permanent magnetic fields at the landing site are $38 \pm 3\ \gamma$ at Apollo 12, 43 ± 6 and $103 \pm 5\ \gamma$ at two Apollo 14 sites separated by 1.1 km, and $6 \pm 4\ \gamma$ at the Apollo 15 site. Table II and Figure 14 list the permanent field components for the Apollo 12 and 15 sites and for the two Apollo 14 sites. The fields are all attributed to remanent magnetization in nearby subsurface material. All field components are expressed in their respective local ALSEP surface coordinate

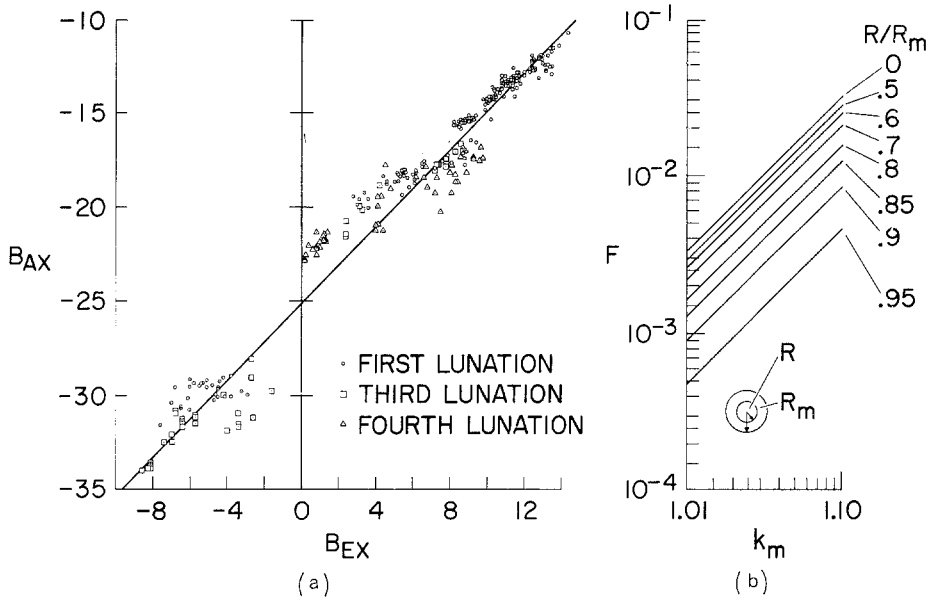

Fig. 13. Graphical representations of Equations (9) and (11). (a) Radial component of Apollo 12 total surface magnetic field B_{Ax} as a function of the radial component of external driving field B_{Ex}. Data points consist of measurements in quiet regions of the geomagnetic tail taken during the first four postdeployment lunations. The B_{Ax} intercept of the least-squares best-fit solid line gives the radial component of the Apollo 12 remanent field; the best-fit slope corresponds to a value of 1.03 ± 0.13 for the bulk relative permeability μ/μ_0 of the Moon. (b) The function F is related to relative magnetic permeability $k_m = \mu/\mu_0$ for various values of R/R_m. R and R_m are internal and external radii, respectively, of a global permeable shell.

TABLE II

Remanent magnetic field measurements at Apollo 15, 14, and 12 sites

Site	Coordinates, deg	Field Magnitude, γ	Magnetic field components, γ Up	East	North
Apollo 15	26.4° N, 3.5° E	6 ± 4	$+4 \pm 4$	$+1 \pm 3$	$+4 \pm 3$
Apollo 14	3.7° S, 17.5° W				
Site A		103 ± 5	-93 ± 4	$+38 \pm 5$	-24 ± 5
Site C′		43 ± 6	-15 ± 4	-36 ± 5	-19 ± 8
Apollo 12	3.2° S, 23.4° W	38 ± 3	-24.4 ± 2.0	$+13.0 \pm 1.8$	-25.6 ± 0.8

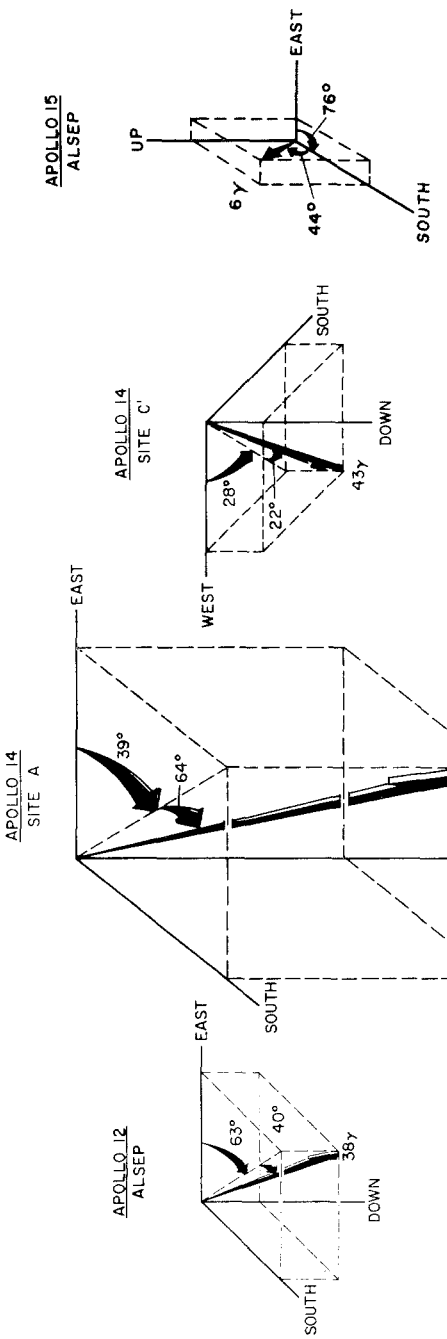

Fig. 14. Magnitudes and orientations of the vector remanent magnetic fields measured at the Apollo 12, 14, and 15 landing sites.

systems ($\hat{x}, \hat{y}, \hat{z}$), which have origins at local deployment sites; each $\hat{x}$ is directed radially outward from the local surface, and $\hat{y}$ and $\hat{z}$ are tangent to the surface and directed eastward and northward, respectively.

1. *Sources of the Remanent Fields*

The three high field readings (at the Apollo 12 and 14 sites) were taken at separations of no more than 185 km, whereas the Apollo 15 reading, taken 1200 km distant, showed a comparatively small field. The large differences between remanent magnetic fields of the Apollo 15 region and of the region common to the Apollo 12 and 14 sites suggest the possibility that the two regions were formed at different times under different ambient field conditions or that the magnetic properties of the materials in the two regions differ substantially. The Apollo 15 measurement, moreover, was obtained on the edge of the Mare Imbrium mascon basin; the fact that little magnetic field exists at that site leads to the preliminary conclusion that mascons are not in general highly magnetic.

The similarities between the Apollo 12 and 14 field measurements (viz., all vectors are pointed down and toward the south and have magnitudes that correspond to within a factor of 3) suggest that the two Apollo 14 sites and possibly the Apollo 12 site are located above a near-surface slab of material that was uniformly magnetized at one time. Subsequently, the magnetization in the slab was altered by local processes, such as tectonic activity or fracturing and shock demagnetization from meteorite impacts. The latter process is graphically illustrated in Figure 15.

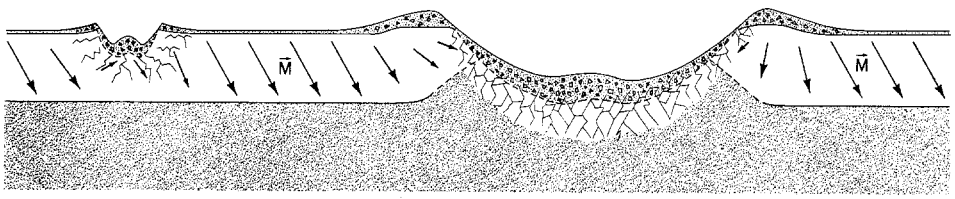

Fig. 15. Conceptional diagram showing disruption of a previously uniformly magnetized subsurface layer by meteorite impact. The vectors (**M**) represent the direction and magnitude of remanent magnetization in the layer.

The Apollo 12 and 14 steady magnetic fields could also originate in surface or subsurface dipolar sources, such as meteoroid fragments or ore bodies. Properties of such a source assumed for the Apollo 12 field have been discussed in a previous work (Dyal and Parkin, 1971a).

Numerous other source models exist that could be postulated for the Apollo 12 and 14 fields. One possibility is that the region was subjected to a uniform magnetic field but that various materials with differing coercivities were magnetized to different strengths. Another model might involve a slow variation in the direction of the magnetizing field, causing regions that passed through the Curie temperature at different times to be magnetized in different directions.

2. *Models for Magnetization of the Remanent Field Sources*

No obvious mechanism for such large scale magnetization of surface materials exists at present. Magnetization of the Apollo 11 and 12 samples would have required an external field greater than 10^3 γ (Helsley, 1970, 1971; Runcorn *et al.*, 1970). Ambient fields of this magnitude have not been measured in space near the Moon; the largest measured so far have been transient fields of a magnitude of approximately 10^2 γ (Dyal *et al.*, 1970b); these transient fields last only a few minutes. It is evident, therefore, that at one time in the lunar past, an ambient field much stronger than at present existed over much or all of the lunar surface. Possible origins of the ancient ambient field could have been external to the Moon (Sun or Earth) or intrinsic to the Moon (e.g., a lunar dynamo).

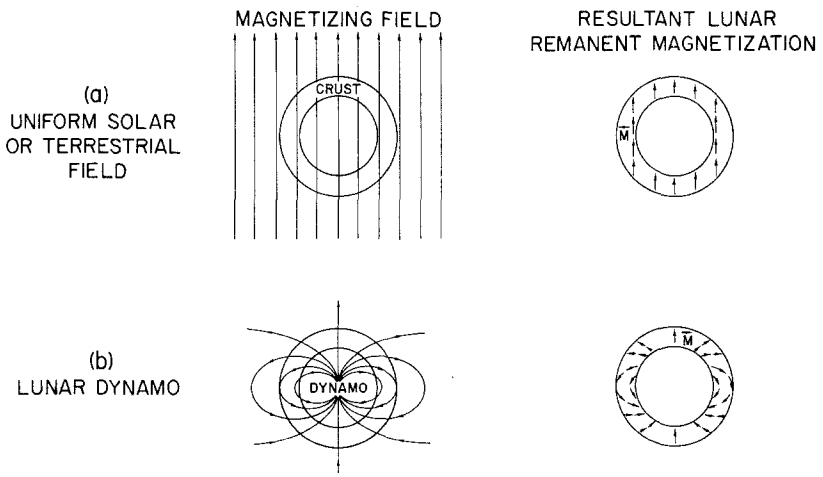

Fig. 16. Possible magnetic events in lunar history as models for magnetization of near surface regions of the Moon. The Moon is shown before and after each hypothetical event. The vectors **M** indicate the direction of remanent magnetization in the crustal region. (a) Magnetization by a strong solar or terrestrial field. (b) Magnetization by a lunar internal dynamo field.

In the high-solar-field model (see Figure 16(a)), the Sun generates a magnetic field, stronger than presently exists, which magnetizes the lunar material. The model requires a solar field of constant direction with respect to the solar and lunar spin axes (e.g., solar dipole moment vector pointed out of the solar ecliptic plane) rather than the present-day sector structure geometry. In the terrestrial field model (Figure 16(a)), the Earth possesses a larger field than in the past, or the Moon has an orbit much closer to the Earth. For a terrestrial field of present-day magnitude, the Moon would have had to approach to within 2 to 3 Earth radii (close to the Roche limit) to be subjected to a 10^3 γ field. An internal lunar dynamo model (Figure 16(b)) requires both a hot core and a sufficient spin rate at the time the surface material cools below the Curie temperature. Past mechanisms for cooling the lunar interior and slowing the

spin rate to the present value are also necessary to the dynamo model. Other possible models include ancient magnetic fields due to thermoelectric currents, eddy currents, and solar wind $\mathbf{v} \times \mathbf{B}$ currents in the Moon.

Preferential selection of any one of the possible models is difficult because available

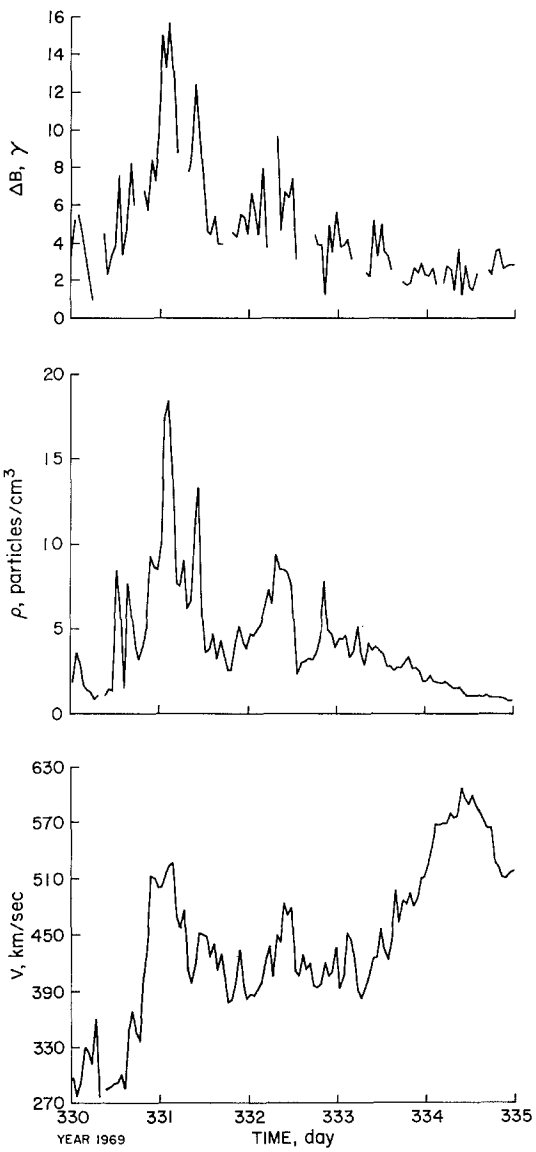

Fig. 17. Simultaneous graphs of magnitude of the vector $\Delta\mathbf{B} = \mathbf{B}_A - (\mathbf{B}_E + \mathbf{B}_S)$, plasma density, and plasma velocity. $\mathbf{B}_A$ is the total surface field measured by the Apollo 12 lunar surface magnetometer, $\mathbf{B}_E$ is the extralunar field measured by lunar orbiting Explorer 35, and $\mathbf{B}_S$ is the remanent field at the Apollo 12 site. Orbital position of the Moon during days 330–335 (Nov. 26–Dec. 1) is shown in Figure 1.

magnetic data represent only a small fraction of the lunar surface. Global mapping of remanent fields by further surface and orbital missions should elucidate the 'magnetic epoch' of lunar history.

C. REMANENT FIELD COMPRESSION BY THE SOLAR WIND

As discussed earlier, Equation (1) reduces to Equation (5) for daytime LSM data in the magnetosheath or free streaming solar wind. Regrouping the field terms, Equation (5) is rewritten as follows:

$$\Delta\mathbf{B} \equiv \mathbf{B}_A - (\mathbf{B}_E + \mathbf{B}_S) = \mathbf{B}_P + \mathbf{B}_F . \tag{12}$$

For frequencies $\leqslant 3 \times 10^{-4}$ Hz, $\mathbf{B}_P$ should approach zero (Sonett *et al.*, 1971; Sill and Blank, 1970); then $\Delta\mathbf{B} = \mathbf{B}_F$, allowing an experimental opportunity to consider the flow field $\mathbf{B}_F$ alone.

If the 38 γ remanent field at the Apollo 12 site is of sufficiently large scale size, a high density solar wind should compress the remanent field (Barnes *et al.*, 1971). To investigate the possibility that the net interaction field $\Delta\mathbf{B} \rightarrow \mathbf{B}_F$ is a field compression phenomenon, plots are shown in Figure 17 for low frequency (1-hr averages) of the vector field difference $\Delta\mathbf{B} = \mathbf{B}_A - (\mathbf{B}_E + \mathbf{B}_S)$, solar wind proton density, and solar wind velocity magnitude measured at the Apollo 12 site. All data are expressed in the surface coordinate system $(\hat{x}, \hat{y}, \hat{z})$ which has its origin at the Apollo 12 magnetometer site; $\hat{x}$ is directed radially outward from the surface while $\hat{y}$ and $\hat{z}$ are tangent to the surface, directed eastward and northward, respectively. Components of the steady remanent field at the Apollo 12 site have been determined to be $B_{Sx} = -24.4\ \gamma$, $B_{Sy} = +13.0\ \gamma$, and $B_{Sz} = -25.6\ \gamma$ (Dyal and Parkin, 1971a). By inspection we see a strong relationship between the magnitude ΔB and plasma density ϱ; no such strong correlation, however, is apparent between ΔB and velocity v alone.

Figure 18 shows the x (vertical), y (easterly), and z (northerly) components of ΔB. Correlation with density is seen in all three components, but it is stronger in the horizontal components y and z and strongest in the z direction. It is noted that each component field change with plasma density has the same polarity as each remanent field component (B_{Sx} and B_{Sz} are negative and B_{Sy} is positive). The correlations between the field difference components ΔB_i and plasma density ϱ therefore suggest that the field change $\Delta\mathbf{B}$ is due to a compression of the local remanent field $\mathbf{B}_S$ by the solar wind, with the largest compression occurring in the z-component. It is possible that ΔB_z shows a greater compression than the other two field components due to the geometric shape of the remanent field. The compression of the remanent field can be investigated further by plotting the energy density increase of the magnetic field ($\Delta B^2/8\pi$) and simultaneous energy density of the solar wind directed normal to the Apollo 12 site ($\varrho m_p v^2 \cos^2 \alpha$ where α is the angle between the average solar wind velocity vector $\mathbf{v}$ and the normal to the lunar surface at the Apollo 12 site). Figure 19 shows that a definite correlation exists between these quantities. There it is concluded that the 38 γ remanent field at the Apollo 12 site is compressed on the lunar sunlit side during times of high solar wind plasma pressure.

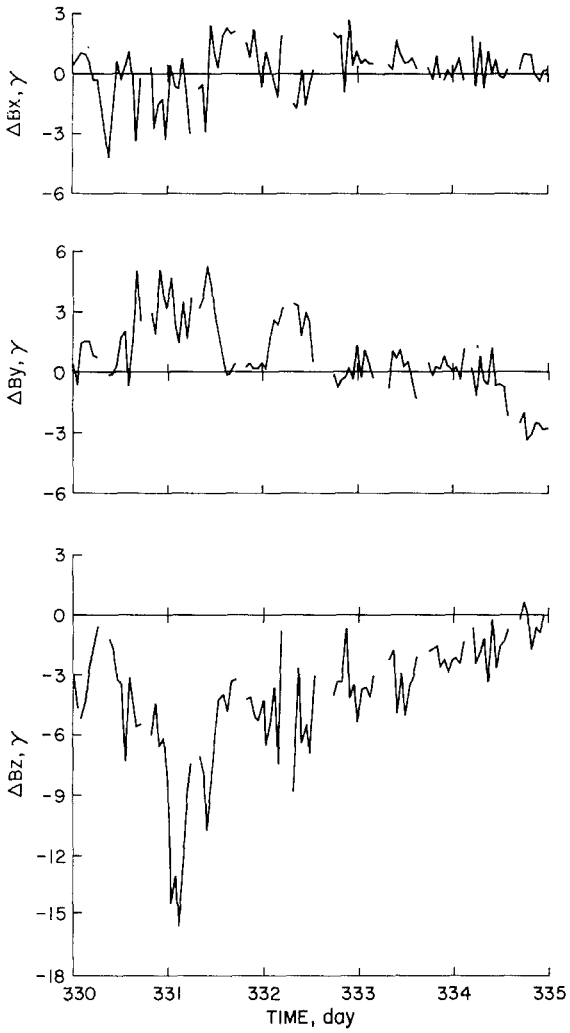

Fig. 18. Components of the magnetic field difference vector **ΔB**. Data are expressed in the surface coordinate system $(\hat{x}, \hat{y}, \hat{z})$ which has its origin at the Apollo 12 magnetometer site; $\hat{x}$ is directed radially outward from the surface while $\hat{y}$ and $\hat{z}$ are tangent to the surface, directed eastward and northward, respectively. The unperturbed steady remanent field at the Apollo 12 site is $\mathbf{B}_S = (-24.4\gamma, +13.0\gamma, -25.6\gamma)$.

6. Summary

A. LUNAR INTERNAL ELECTRICAL CONDUCTIVITY

The electrical conductivity of the lunar interior has been determined from magnetic field step transient measurements made on the lunar dark side. The data fit remarkably close to the classical theory of a conducting sphere in a magnetic field. Radial and tangential magnetic-field component measurements indicate a global rather than a local response to these step transients. The simplest model which qualitatively explains

the dark-side transient-response data is a spherically symmetric three-layer model having a nonconducting outer crust of radial thickness $\approx 0.03\ R_{\text{moon}}$. An intermediate layer, of radial thickness $\Delta R \approx 0.37\ R_{\text{moon}}$, has electrical conductivity $\sigma_1 \approx 3.5 \times 10^{-4}$ mhos/m; the inner core has radius $R_z \approx 0.6\ R_{\text{moon}}$ and conductivity $\sigma_z \approx 10^{-2}$ mhos/m. Electrical conductivities calculated for the three-layer model are related to the

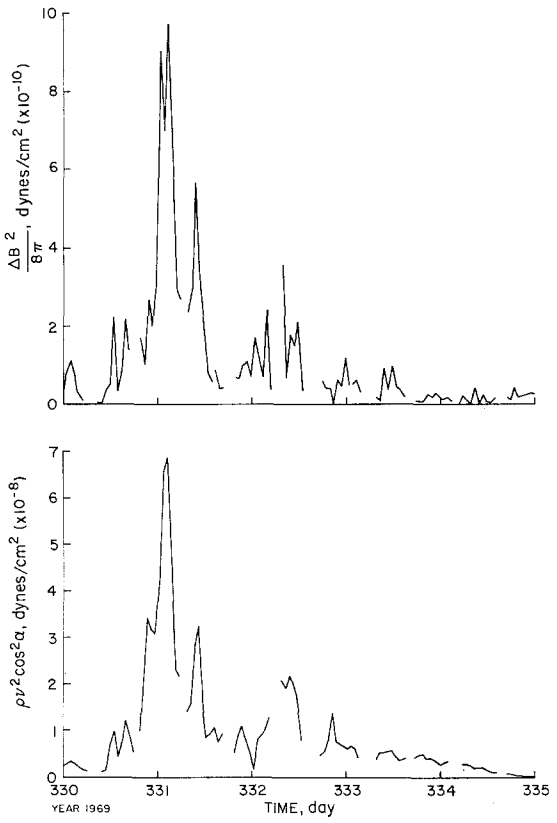

Fig. 19. Simultaneous plots of the magnetic field pressure difference $\Delta B^2/8\pi$ and solar wind pressure normal to the Apollo 12 surface site, showing the correlation between the pressures. The angle is the angle between the solar wind velocity v and the normal to the lunar surface ($-\hat{x}$) at the Apollo 12 site.

temperatures in the three regions. For the example of an olivine Moon, the temperatures of the layers are as follows: Crust, <440 K; intermediate layer, ≈ 890 K; core, ≈ 1240 K.

B. RELATIVE MAGNETIC PERMEABILITY OF THE LUNAR INTERIOR

The whole-moon relative permeability has been calculated from field measurements to be $\mu/\mu_0 = 1.03 \pm 0.13$. If the inner core of radius $R \approx 0.6\ R_m$ has a Curie temperature <1240 K, then $\mu/\mu_0 = 1.05 \pm 0.14$ is determined for the outer layer.

C. REMANENT MAGNETIC FIELDS AT THE APOLLO SITES

The measured remanent magnetic fields measured to date on the Moon are $38 \pm 3\ \gamma$ at Apollo 12 in Oceanus Procellarum; 103 ± 5 and $43 \pm 6\ \gamma$ at two Apollo 14 sites separated by 1.1 km in Fra Mauro; and $6 \pm 4\ \gamma$ at the Apollo 15 Hadley-Apennines site.

Simultaneous measurements by the lunar orbiting Explorer 35 satellite have shown that the sources of these remanent fields are not global in extent. The Apollo 12 remanent field, if a single dipolar source, must be confined to a region within 200 km of the landing site. Gradient measurements and the extent of compression of this remanent field place a lower bound of 2 km for the scale size of the Apollo 12 field source (Barnes *et al.*, 1971). Possible origins of the large ancient ambient field required to magnetize the remanent sources could have been external to the Moon (Sun or Earth) or intrinsic to the Moon (e.g., a lunar dynamo).

D. REMANENT FIELD COMPRESSION BY THE SOLAR WIND

Measurements show that the remanent field at the Apollo 12 site is compressed by the solar wind. The 38-γ remanent field is compressed to 54 γ by a solar-wind pressure increase of 7×10^{-8} dynes/cm^2. The change in magnetic pressure is proportional to the change in plasma pressure and the field is compressed primarily in the z (northerly) component. This compression asymmetry is perhaps caused by asymmetries in the remanent field geometry.

Acknowledgments

The authors wish to express their appreciation to Drs. C. P. Sonett and D. S. Colburn of NASA-Ames Research Center for their help and use of Explorer 35 data and to Drs. C. W. Snyder and D. R. Clay of the Jet Propulsion Laboratory for the use of Apollo 12 solar wind spectrometer data.

References

Barnes, A., Cassen, P., Mihalov, J. D., and Eviatar, A.: 1971, *Science* **172**, 716–718.

Dyal, P. and Parkin, C. W.: 1971a, in *Proceedings of the Second Lunar Science Conference* **3**, (ed. by A. A. Levinson), MIT Press, Cambridge, Mass., pp. 2391–2413.

Dyal, P. and Parkin, C. W.: 1971b, *J. Geophys. Res.* **76**, 5947–5969.

Dyal, P., Parkin, C. W., and Sonett, C. P.: 1970a, *IEEE Trans. on Geoscience Electronics* **GE-8**, 203–215.

Dyal, P., Parkin, C. W., and Sonett, C. P.: 1970b, 'Lunar Surface Magnetometer Experiment', in Apollo 12 Preliminary Science Report, NASA SP-235, pp. 55–73.

Dyal, P., Parkin, C. W., Sonett, C. P., DuBois, R. L., and Simmons, G.: 1971, 'Lunar Portable Magnetometer Experiment', in *Apollo 14 Preliminary Science Report*, NASA SP-272, pp. 227–237.

England, A. W., Simmons, G., and Strangway, D.: 1968, *J. Geophys. Res.* **73**, 3219–3226.

Geyger, W. A.: 1964, *Nonlinear-Magnetic Control Devices*, McGraw-Hill, New York.

Gordon, D. E., Lundsten, R. H., and Chiarodo, R. A.: 1965, *IEEE Trans. on Magnetics*, **MAG-1**, 330–337.

Helsley, C. E.: 1970, in *Proceedings of the Apollo 11 Lunar Science Conference*, (ed. by A. A. Levinson) **3**, Pergamon, New York, pp. 2213–2219.

Helsley, C. E.: 1971, in *Proceedings of the Second Lunar Science Conference* **3** (ed. by A. A. Levinson), MIT Press, Cambridge, Mass., pp. 2485–2490.

Jackson, J. D.: 1962, *Classical Electrodynamics*, John Wiley, New York, 163.

Keller, G. V. and Frischknecht, F. C.: 1966, *Electrical Methods in Geophysical Prospecting*, Pergamon, New York.

Kopal, Z.: 1969, *The Moon*, D. Reidel, Dordrecht, The Netherlands.

Nagata, Takesi: 1970, 'Electrical Conductivity and Age of the Moon', Paper M. 14, Thirteenth Planetary Meeting, COSPAR, Leningrad, U.S.S.R.

Runcorn, S. K., Collinson, D. W., O'Reilly, W., Battey, M. H., Stephenson, A. A., Jones, J. M., Manson, A. J., and Readman, P. W.: 1970, *Proceedings of Apollo 11 Lunar Science Conference* **3**, Pergamon, New York, pp. 2369–2387.

Sill, W. R. and Blank, J. L.: 1970, *J. Geophys. Res.* **72**, 501.

Smythe, W. R.: 1950, *Static and Dynamic Electricity*, McGraw-Hill, New York.

Snyder, C. W., Clay, D. R., and Neugebauer, M.: 1970, in *Apollo 12 Preliminary Science Report*, NASA SP-235, pp. 75–81.

Sonett, C. P., Colburn, D. S., Currie, R. G., and Mihalov, J. D.: 1967, in *Physics of the Magnetosphere* (ed. by R. L. Carovillano, J. F. McClay, and H. R. Radoski), D. Reidel, Dordrecht, The Netherlands.

Sonett, C. P., Schubert, G., Smith, B. F., Schwartz, K., and Colburn, D. S.: 1971, in *Proceedings of the Second Lunar Science Conference* **3**, (ed. by A. A. Levinson), MIT Press, Cambridge, Mass., pp. 2415–2431.

Urey, H. C. and MacDonald, G. J. F.: 1970, in *Physics and Astronomy of the Moon* (ed. by Z. Kopal), Academic Press, New York.